

# Multi-beam Antenna Combining for 28 GHz Cellular Link Improvement in Urban Environments

Shu Sun

NYU WIRELESS

Polytechnic Institute of New York University, Brooklyn,  
NY 11201 USA  
ss7152@nyu.edu

Theodore S. Rappaport

NYU WIRELESS

Polytechnic Institute of New York University, Brooklyn,  
NY 11201 USA  
tsr@nyu.edu

**Abstract**—This article demonstrates the performance of multi-beam antenna combining for improving link quality in future millimeter-wave cellular systems. Using experimental data obtained from 28 GHz propagation measurements in New York City [8], we demonstrate how the combination of two, three and four beams, either noncoherently or coherently at the mobile receiver antenna, can improve the propagation link substantially. The results reveal that an average of 28.1 dB improvement in path loss can be achieved via combining the strongest four received signals coherently, when compared to the case of randomly received signals using a single beam at the receiver. This paper is the first to present the potential of multi-beam combining for improving link budget (e.g., extending range) in future mm-wave urban cellular systems.

**Keywords**—*beam combining; beamforming; 28 GHz; millimeter wave propagation; 5G; cellular; mobile communications; mm-wave; MIMO*

## I. INTRODUCTION

Smart antenna technologies have been widely explored, as they can improve the performance and capacity of wireless systems [1]. Multiple-Input Multiple-Output (MIMO) uses multiple antennas at both the transmitter (TX) and receiver (RX), and is a popular form of smart antenna technologies. MIMO systems have been a vital part in modern wireless communication applications and standards such as IEEE 802.11n, WiMAX, 3GPP Long Term Evolution (LTE) and 4G. One of the most prominent merits of MIMO is that it allows the implementation of beamforming. Utilizing directional antennas or MIMO at both the handset and base station exploits the spatial degrees of freedom in the propagation channel, and could improve link margin in the most densely populated propagation environments. When sufficient diversity and link margin exists, MIMO can offer substantial increases in throughput over conventional antenna diversity methods, and is now a part of 4G LTE.

Recently, the concept of millimeter-wave (mm-wave) cellular has been gaining interest for use in 5<sup>th</sup> generation cellular, where many GHz of spectrum could be used to offer orders of magnitude higher data rates to mobile users, while also supporting backhaul between small cells. At these frequencies, where the available spectrum is unprecedented, the smaller wavelengths enable high-gain steerable multi-

element antennas to be fabricated and mounted on small handset devices as well as on small base stations [2][3][9][10][11].

Beamforming at the base station significantly increases the signal-to-interference ratio (SIR) at the target mobile receiver, which can be implemented using fixed or adaptive codebooks. On the other hand, the received signal quality will be further enhanced if the signal power at the receiver can be combined using a phased array capable of combining energy from multiple beams simultaneously. To date, cellular beam combining has been investigated primarily for cellular CDMA systems, where RAKE receivers align the received signal in multiple beams and combine the signal energy for signal-to-noise ratio (SNR) enhancement [4][5][6], where capacity evaluations are often performed by computer simulation, without the benefit of experimental results from real world channels.

This paper presents new results that consider the improved propagation using multi-beam combining, based on 28 GHz propagation measurements for outdoor cellular wireless communication channels in New York City [8]. By assuming the existence of a receiver that can perform either noncoherent or coherent multi-beam combining, we demonstrate the actual improvements in link margin for urban mm-wave cellular channels. These early results provide a sense of achievable improvements in path loss (i.e. link budget) through beam combining that could be expected in futuristic mm-wave femtocells for future 5<sup>th</sup> generation (5G) cellular communication systems.

## II. EXPERIMENT PROCEDURE

### A. Measurement Procedure

28 GHz propagation measurements were conducted at three TX and 25 RX measurement locations (yielding 75 unique TX-RX location combinations) around the NYU campus in Manhattan, New York City, using a 400 Mega-chip-per-second (Mcps) sliding correlator channel sounder with a slide factor of 8000, and 24.5 dBi (10.9<sup>o</sup> beamwidth) rotatable directional horn antennas at both the TX and RX. At each RX location, 10 antenna pointing angle configurations (where a configuration denoted particular uptilt or downtilt angles for the TX and RX elevation angles) were used, and

extensive multipath power measurements were carried out for each configuration. The related measurement procedure is detailed in [8]. For nine of the ten configurations, the base station TX antenna pointing angle was fixed so as to obtain the maximum power at the ground-level RX, while the RX antenna was sequentially rotated throughout the 360° azimuth plane in 10° angular segments (a 10° angular segment is a particular antenna pointing angle with 10° azimuthal angle spread), i.e. 36 antenna pointing angles over the azimuth. For the tenth configuration, the RX antenna angle was fixed to point where the maximum power was obtained, and the TX antenna was sequentially rotated over the complete azimuth plane in 36 angular segments. Power Delay Profiles (PDPs) were recorded at every azimuth angle and for each configuration and subsequent data processing was performed to obtain the corresponding received power and channel statistics [8][12].

### B. Beam Combining Procedure

In this article, beam combining considers combining the received powers that were recorded from different 10° angular segments measured at a particular RX location. Future work will use the data to create statistical models for arbitrary antenna arrays, but for this paper, we focus on measured results using 10° beamwidth antennas. Using the measured data, we then consider the potential improvement resulting from both coherent and noncoherent reception at the RX. For coherent reception, we assume that the received powers from each of the best beam headings of interest are combined using known carrier phase information (this results in optimal/maximum power from each of the combined beams), while noncoherent reception is considered by simply adding (linearly) the powers received from each beam heading without considering phase information. This non-coherent approach is based on the reasonable assumption that the incoming phases of each received signal in each beam is uniformly and identically, independently distributed (iid) so that the powers can simply be added [7]. Note that we do not assume alignment or equalization of individual multipath delays from each of the individual beams, but simply compute received power at each location as the area under the PDP, as current OFDM and very wideband modulation methods equalize out multipath. Thereby, focusing on the powers from different beams provides good first order insight into the potential improvement in link coverage that might be obtained from beam combining.

The measured NYC data occupies over 100 Gigabytes [8], hence computer (and not manual) inspection of all PDP measurements for all antenna pointing angle combinations at each of the individual RX locations was needed to find the PDPs and their corresponding antenna pointing angles that provided the strongest (i.e. smallest path loss), second strongest, third strongest, and the fourth strongest received signals at each RX location. For each RX location, all ten antenna configurations were considered, which is reasonable since adaptive antennas will be employed at both the TX and RX in mm-wave cellular systems [2][10][11]. The single

strongest, the first and second strongest, the first three strongest, and the first four strongest power levels from the measured PDPs over all of the different pointing angles at each RX location were then combined either coherently or noncoherently, and the results for path loss over all RX locations were observed. For the case of coherent beam combining, the square root of the absolute (i.e. linear) received power levels in Watts were computed, and the voltages obtained at the strongest few 3D (three dimensional) angular segments were summed, thus the total coherent voltage was found at each RX location, and then this value was squared to obtain received power in units of Watts, which was then converted into dBm. To compute noncoherent power, each of the strongest received powers was converted from dBm to its linear value in Watts, and summed directly. The total noncoherent power value was then converted back to dBm. Eqns. (1) and (2) illustrate the approaches of calculating the total received coherent ( $P_C$ ) and noncoherent ( $P_{NC}$ ) powers at each RX using the combination of the N strongest beams, respectively:

$$P_C = (\sum_{i=1}^N \sqrt{P_i})^2 \quad (1)$$

$$P_{NC} = \sum_{i=1}^N P_i \quad (2)$$

where  $P_C$  and  $P_{NC}$  denote the coherently and noncoherently combined powers in Watts, respectively.  $P_i$  ( $i=1,2,\dots,N$ ) represents the  $i^{\text{th}}$  strongest received power (in Watts).

By employing the resulting obtained received power from beam combining, the corresponding path loss was calculated. Finally, scatter plots of path loss (PL) versus TX-RX separation were generated.

Since the measurements provided no absolute phase information, the assumption of absolute phase must be made, which is a reasonable assumption for coherent modulation that would be implemented in commercial mm-wave cellular systems. Coherent combining is expected to provide superior improvement in SNR as compared to noncoherent methods, and 3dB improvement is a general rule of thumb for equal-gain paths.

### III. RESULTS AND ANALYSIS

Path loss (in dB) usually has a linear relationship with logarithmic distance, which can be expressed by the following equation:

$$\overline{PL}(d)[\text{dB}] = \beta \cdot 10 \log_{10}(d) + \alpha \quad (3)$$

where  $\overline{PL}(d)$  (in dB) denotes the average path loss taken over all antenna pointing angles at a TX-RX separation of  $d$  (in meters),  $\beta$  is the linear slope, and  $\alpha$  is the floating intercept in dB [13]. Path loss is essential in studying link budget and system capacity, as the higher the path loss, the greater the attenuation of the propagating signal (i.e. this sets the limit on range from a base station, determines interference from neighboring cells, and plays a major role in determining infrastructure investment).

In (3),  $\overline{PL}(\bar{d})$  (in dB) is obtained by the least-square linear regression fit, in which the linear slope  $\beta$  can be derived as below:

$$\beta = \frac{\sum_i^n (d_i - \bar{d}) \cdot (PL_i - \overline{PL})}{\sum_i^n (d_i - \bar{d})^2} \quad (4)$$

where  $n$  denotes the total number of measurement snapshots,  $d_i$  is the distance of the  $i^{\text{th}}$  measurement snapshot in logarithmic scale,  $\bar{d}$  indicates the average distance of all measurement snapshots in logarithmic scale, which is obtained by converting all  $d_i$ 's from linear scale (in meters) to logarithmic scale and then finding the average distance in logarithmic scale.  $PL_i$  (in dB) is the path loss value of the  $i^{\text{th}}$  measurement snapshot, and  $\overline{PL}$  (in dB) is the average path loss value over all measurement snapshots.

The floating intercept  $\alpha$  can be derived by:

$$\alpha(\text{dB}) = \overline{PL}[\text{dB}] - \beta \cdot \overline{10 \log_{10} d} \quad (5)$$

where  $\alpha$  is denoted over a specific range of distances (30 m – 200 m in our case) based on measured locations and resulting path losses. The regression fit is performed for all 26 NLOS TX-RX location combinations where a signal was recorded.

Shadow fading (SF, or shadowing) is another factor influencing path loss, which is caused by the surrounding environmental clutter [7] and thus expected to be larger in dense urban environment such as NYC. SF is generally expressed as a zero-mean Gaussian random variable  $X_{\text{SF}}$  with standard deviation  $\sigma_{\text{SF}}$  (in log scale) about  $\overline{PL}(\bar{d})$  in Eqn(3). Therefore, the total path loss due to attenuation and SF in the channel can be described as follows:

$$PL(D) [\text{dB}] = \overline{PL}(\bar{d})[\text{dB}] + X_{\text{SF}}[\text{dB}] \quad (6)$$

where  $PL(D)$  represents the total path loss (a random variable),  $\overline{PL}(\bar{d})$  is the path loss due to attenuation, and  $X_{\text{SF}}$  is due to shadowing.

Measurements from [8] provided angle of arrival (AOA) and angle of departure (AOD) data for multipath angular spread analysis. By completing a 360° exhaustive sweep of the TX and RX antennas in 10° steps, the angles with the highest received power were determined by observing PDPs. Fig. 1 demonstrates a polar plot of received power at the RX on the corner of Greene and Broadway in downtown Manhattan in a NLOS environment [8]. The distance between the TX and RX was 78 m. In the figure, each dot represents one 10° angular segment, and corresponds to the received power level in dBm (denoted on the radius) at the RX azimuth angle. The number of resolvable multipath components, path loss in dB with respect to a 5 m free space reference, and RMS delay spread in nanoseconds are displayed from left to right on the periphery of the plot. As can be observed, power was received at 22 out of 36 RX azimuth angles, which indicates that a plethora of multipath components exist at different antenna pointing angles. Fig. 2 shows the PDPs of the four strongest received

signals contained in different beams. The diverse multipath beams can be utilized for beam combining.

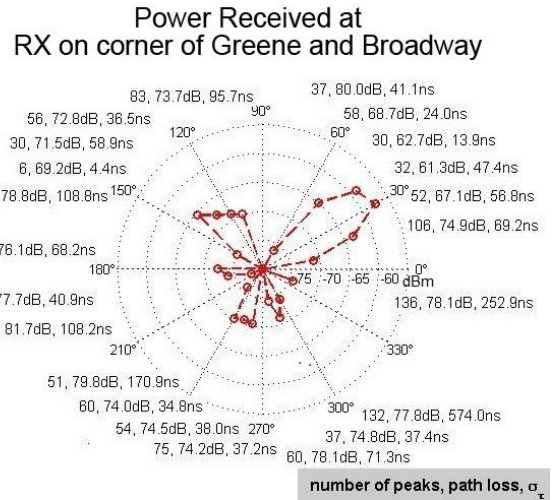
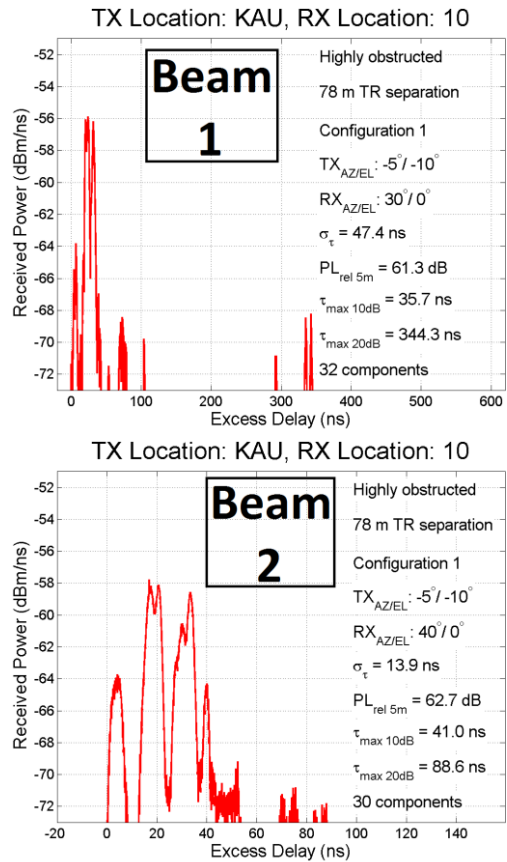


Fig. 1. Polar plot showing the received power at a NLOS location at 28 GHz. This plot shows an AOA measurement at the RX on Greene and Broadway from the TX on the five-story Kaufman building (78 m TX-RX separation). The polar plot shows the received power in dBm, the number of resolvable multipath components, the path loss in dB with respect to the 5 m free space reference, and RMS delay spread with specific RX azimuth angles [8].



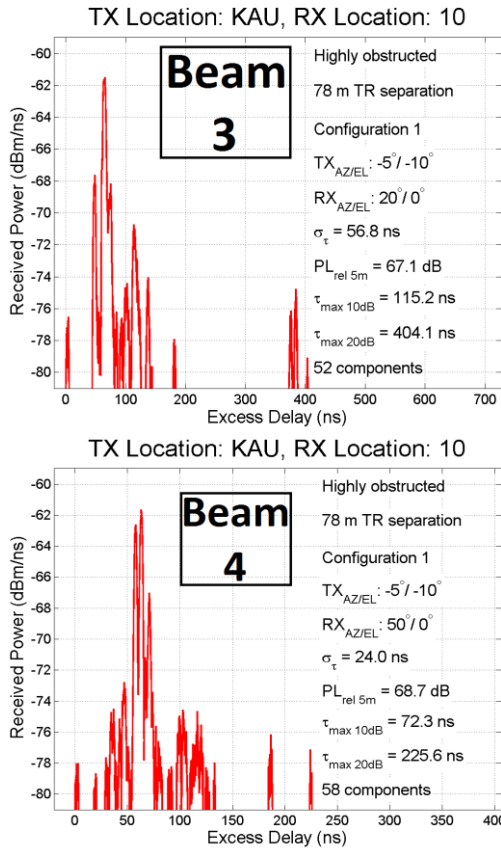


Fig. 2. PDPs of incident beams containing the three strongest received powers identified in Fig. 1 at 28 GHz in a NLOS environment in Manhattan using 24.5 dBi horn antennas at both TX and RX.

Five scatter plots of path loss versus distance (TX-RX separation) were produced from our measured data in Manhattan. Among the 28 TX-RX location combinations where signals were acquired, two were LOS case and the remaining 26 were NLOS case. Since the LOS case provides very close to free space path loss, which is often the best case for urban propagation channels, only the more challenging NLOS measurements are considered in this paper. The relationship between path loss and TX-RX separation, as well as regression fit path loss results corresponding to all uncombined received signals, the best (e.g. strongest) received signal over all angular segments in 3D at each RX, the best two combined signals, the best three combined signals, and the best four combined signals are displayed in Figs. 3-7. Table I shows the received power and improvement in path loss from various beam combining combinations over all NLOS locations, and the overall average improvement.

It can be summarized from Figs. 3-7 that the average path loss at a certain distance drops monotonically as the number of combined signals increases from one to four for both noncoherent and coherent combinations of beams. For instance, the path loss at 30 m TX-RX separation corresponding to four coherently combined signals improved by about 10 dB compared to that of using the single best beam. It is also worth noting that for a fixed number of combined beams, the path loss for coherent combining is

always at least  $\sim 3$  dB better (i.e. smaller) than for the noncoherent case, showing the dramatic improvement that can be achieved using coherent power combining over the best few received beams in 3D. For example, in the case of combining four signals coherently, the path loss decreases by 5.9 dB, on average, with respect to that of noncoherent combining of four beams, as can be observed from the last row of Table I. This is not surprising, as coherent combination of in-phase signals gives rise to the strongest power compared with noncoherent combination and non in-phase coherent combination, yet this is the first known data of this type for mm-wave cellular. The results are important, since an improvement of 5.9 dB in average path loss results in a cell radius coverage range increase of 41% compared to a single beam RX in a  $n=4$  propagation environment. Furthermore, the improvement in path loss when combining the best two beams *coherently* (22.8 dB above arbitrary single beam pointing) is even more conspicuous than that of combining the best four beams *noncoherently* (22.2 dB), thus showing *coherent* combining of fewer antennas easily justifies the receiver complexity. Note that shadow fading is only slightly reduced from about 8.97 dB to 8.86 dB with the addition of combined signals. Comparing the improvement in path loss for the case of coherent combining for the four strongest beams, and that of just a single strongest beam, it can be observed that the average improvement in link budget goes from 17.5 dB up to 28.1dB, yielding 10.6 dB improvement, which is remarkably significant to carriers (80% range extension for  $n=4$ ).

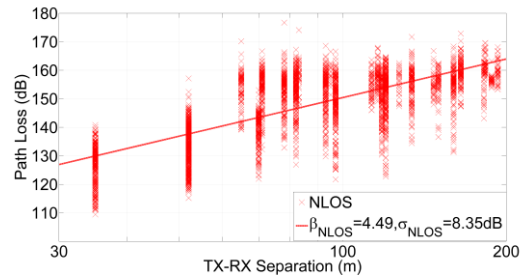


Fig. 3. Measured path loss versus TX-RX separation for 28 GHz outdoor cellular channels in NYC. The red crosses represent measured path loss values obtained from PDPs, and the red line denotes least-square fit through the path losses. The slope of the red line is 4.49, while the shadow fading factor is 8.35 dB.

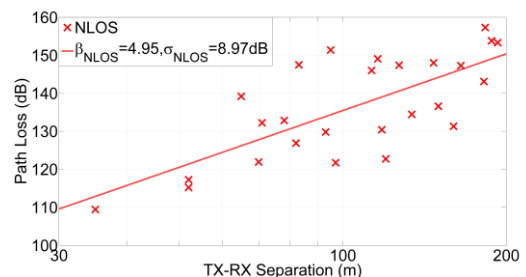


Fig. 4. Path loss versus TX-RX separation at 28 GHz in NYC for the best (i.e. strongest) signal at each RX location. The red crosses represent path loss values, and the red line denotes least-square fit through the path losses. The slope of the red line is 4.95, while the shadow fading factor is 8.97 dB.

Table I: TX-RX separation, average received power ( $P_{av}$ ), received power of the best single signal – i.e. from the single best antenna pointing angle ( $P_{C1}$  or  $P_{NC1}$ ), received power of the best two, three, and four signals combined noncoherently (denoted by  $P_{NC2}$ ,  $P_{NC3}$ ,  $P_{NC4}$  respectively), received power of the best two, three, and four signals combined coherently (denoted by  $P_{C2}$ ,  $P_{C3}$ ,  $P_{C4}$  respectively), and the corresponding improvement in path loss compared to the average received power at each RX location.

RX	TX-RX Separation (m)	$P_{av}$ (dBm)	$P_{C1}$ (or $P_{NC1}$ ) (dBm)	Improve-ment in Path Loss (dB)	Noncoherent Combining					Coherent Combining						
					$P_{NC2}$ (dBm)	Improve-ment in Path Loss (dB)	$P_{NC3}$ (dBm)	Improve-ment in Path Loss (dB)	$P_{NC4}$ (dBm)	Improve-ment in Path Loss (dB)	$P_{C2}$ (dBm)	Improve-ment in Path Loss (dB)	$P_{C3}$ (dBm)	Improve-ment in Path Loss (dB)	$P_{C4}$ (dBm)	Improve-ment in Path Loss (dB)
1	78	-73.8	-53.8	20.0	-52.0	21.8	-50.8	23.0	-49.9	23.9	-49.1	24.7	-46.1	27.7	-44.0	29.8
2	52	-54.9	-38.3	16.6	-35.5	19.4	-33.9	21.0	-32.8	22.1	-32.5	22.4	-29.2	25.7	-26.8	28.1
3	116	-78.8	-70.0	8.8	-67.4	11.4	-66.1	12.7	-65.1	13.7	-64.4	14.4	-61.3	17.5	-59.1	19.7
4	65	-74.4	-60.2	14.2	-57.2	17.2	-55.7	18.7	-54.6	19.8	-54.2	20.2	-50.9	23.5	-48.6	25.8
5	83	-79.3	-68.5	10.8	-65.9	13.4	-64.5	14.8	-63.7	15.6	-62.9	16.4	-59.7	19.6	-57.7	21.6
6	183	-83.1	-78.3	4.8	-75.5	7.6	-74.0	9.1	-73.0	10.1	-72.5	10.6	-69.2	13.9	-67.0	16.1
7	165	-80.5	-68.3	12.2	-65.3	15.2	-63.6	16.9	-62.6	17.9	-62.3	18.2	-58.9	21.6	-56.6	23.9
8	118	-71.3	-51.4	19.9	-48.6	22.7	-47.1	24.2	-46.1	25.2	-45.6	25.7	-42.4	28.9	-40.1	31.2
9	188	-77.6	-74.8	2.8	-72.0	5.6	-70.5	7.1	-69.4	8.2	-69.0	8.6	-65.7	11.9	-63.4	14.2
10	70	-60.3	-42.9	17.4	-40.4	19.9	-39.0	21.3	-38.1	22.2	-37.5	22.8	-34.2	26.1	-32.1	28.2
11	35	-47.6	-30.4	17.2	-28.1	19.5	-26.6	21.0	-25.6	22.0	-25.1	22.5	-21.9	25.7	-19.6	28.0
12	71	-74.8	-53.2	21.6	-50.9	23.9	-50.1	24.7	-49.5	25.3	-47.9	26.9	-45.5	29.3	-43.8	31.0
13	82	-73.7	-47.9	25.8	-46.1	27.6	-44.9	28.8	-44.1	29.6	-43.2	30.5	-40.2	33.5	-38.2	35.5
14	113	-75.4	-67.0	8.4	-64.0	11.4	-62.8	12.6	-61.8	13.6	-61.0	14.4	-58.0	17.4	-55.8	19.6
15	97	-70.3	-42.7	27.6	-41.1	29.2	-39.9	30.4	-39.0	31.3	-38.2	32.1	-35.3	35.0	-33.2	37.1
16	150	-76.1	-57.6	18.5	-55.6	20.5	-54.5	21.6	-53.6	22.5	-52.7	23.4	-49.8	26.3	-47.8	28.3
17	182	-77.8	-64.1	13.7	-62.2	15.6	-61.2	16.6	-60.5	17.3	-59.3	18.5	-56.6	21.2	-54.7	23.1
18	95	-79.7	-72.4	7.3	-70.5	9.2	-69.4	10.3	-68.6	11.1	-67.6	12.1	-64.8	14.9	-62.8	16.9
19	52	-53.6	-36.2	17.4	-34.1	19.5	-33.3	20.3	-32.6	21.0	-31.2	22.4	-28.7	24.9	-26.9	26.7
20	93	-73.4	-50.8	22.6	-48.4	25.0	-47.3	26.1	-46.5	26.9	-45.4	28.0	-42.6	30.8	-40.6	32.8
21	120	-72.9	-43.7	29.2	-41.0	31.9	-39.6	33.3	-38.6	34.3	-38.0	34.9	-34.8	38.1	-32.6	40.3
22	147	-75.8	-69.0	6.8	-66.6	9.2	-65.0	10.8	-64.0	11.8	-63.6	12.2	-60.3	15.5	-58.0	17.8
23	134	-75.1	-55.4	19.7	-52.9	22.2	-51.4	23.7	-50.6	24.5	-49.9	25.2	-46.6	28.5	-44.6	30.5
24	160	-75.9	-52.3	23.6	-49.5	26.4	-48.0	27.9	-47.3	28.6	-46.5	29.4	-43.2	32.7	-41.4	34.5
25	193	-80.5	-74.3	6.2	-71.3	9.2	-69.8	10.7	-68.7	11.8	-68.3	12.2	-65.0	15.5	-62.7	17.8
26	127	-77.0	-68.4	8.6	-65.7	11.3	-64.1	12.9	-63.0	14.0	-62.7	14.3	-59.4	17.6	-57.0	20.0
<b>Average Improvement in path loss (dB)</b>				17.5	19.8		21.2		22.2		22.8		25.9		28.1	

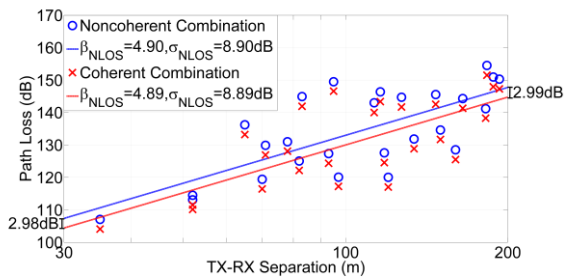


Fig. 5. Path loss versus TX-RX separation at 28 GHz in NYC for the best (i.e. strongest) two signals combined noncoherently and coherently at each RX location. The blue circles and red crosses represent path loss values for noncoherent combination and coherent combination, respectively. The blue and red lines denote least-square fit through the path losses. The slopes of the blue and red lines are 4.90 and 4.89, while the shadow fading factors are 8.90 dB and 8.89 dB, respectively.

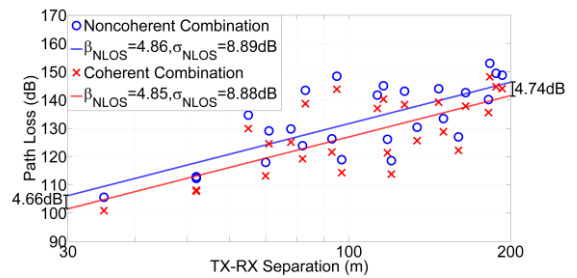


Fig. 6. Path loss versus TX-RX separation at 28 GHz in NYC for the best (i.e. strongest) three signals combined noncoherently and coherently at each RX location. The blue circles and red crosses represent path loss values for noncoherent combination and coherent combination, respectively. The blue and red lines denote least-square fit through the path losses. The slopes of the blue and red lines are 4.86 and 4.85, while the shadow fading factors are 8.89 dB and 8.88 dB, respectively.

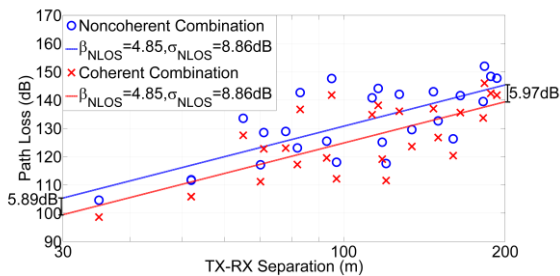


Fig. 7. Path loss versus TX-RX separation at 28 GHz in NYC for the best (i.e. strongest) four signals combined noncoherently and coherently at each RX location. The blue circles and red crosses represent path loss values for noncoherent combination and coherent combination, respectively. The blue and red lines denote least-square fit through the path losses. The slopes of the blue and red lines are both 4.85, while the shadow fading factors are both 8.86 dB.

Since coherent beam combining exerts striking effects on the received signal quality and link budget, it is desirable to adopt coherent beam combining in cellular communication systems. RAKE receivers, which combine the multipath components from each fingers, can be used to implement coherent beam combining. As RAKE combiners require pilot symbols to estimate the channel impulse response, the receiver complexity seems to be aggravated. Nevertheless, as mentioned above, the performance of coherent combining of fewer antennas surpasses that of noncoherent combining, which relieves the system complexity. Moreover, RAKE receivers with smart antennas are feasible in a wide variety of radio devices including mobile handsets due to validated antennas diversity gain [14].

#### IV. CONCLUSION

We have presented the impact of noncoherent and coherent bi-beam, tri-beam and quad-beam combining on path loss and shadow fading, employing the experimental data obtained in the 28GHz outdoor propagation measurements in New York City in 2012. The results show that beam combining can significantly improve signal quality, and decrease path loss and shadow fading, which leads to better signal coverage and link margin for carriers. Particularly, combining the four strongest beams coherently yields more than 28 dB of link budget improvement over arbitrarily pointed beams, and 10.6 dB of improvement when compared to a single optimum beam over typical cellular distances. This works shows promise for adaptive beamforming algorithms and high gain phased antenna arrays for the development of future mm-wave cellular communication systems.

#### ACKNOWLEDGMENT

This work was sponsored by Samsung DMC R&D Communications Research Team (CRT), Intel, and National

Science Foundation (NSF). The authors thank George R. MacCartney, Mathew Samimi, Junhong Zhang, Shuai Nie, Yuanpeng Liu and Dr. Sundeep Rangan of NYU WIRELESS for their contributions to this project. The authors also thank the NYU administration, NYU Public Safety, and NYPD for their support of the measurements. The measurements were conducted under U.S. FCC Experimental License 0040-EX-ML-2012.

#### REFERENCES

- [1] Winters, J. H., "Smart antennas for wireless systems," *Personal Communications, IEEE*, vol.5, no.1, pp.23-27, Feb. 1998.
- [2] Kao-Cheng Huang, Edwards, D.J., "60 GHz Multibeam Antenna Array for Gigabit Wireless Communication Networks," *IEEE Transactions on Antennas and Propagation*, vol.54, no.12, pp.3912-3914, Dec. 2006.
- [3] Ranvier, S., Kivinen, J., Vainikainen, P., "Millimeter-Wave MIMO Radio Channel Sounder," *Instrumentation and Measurement, IEEE Transactions on*, vol.56, no.3, pp.1018-1024, June 2007.
- [4] Sano, H., Murai, H., Miyake, M., "Performance of beam-combining scheme for DS-CDMA using weighting factor based on interference level," *IEEE VTS 50th*, vol.2, pp.993-997, Sep. 1999.
- [5] Hara, Y., Yonezawa, R., and Chiba, I., "On the capacity of Cellular CDMA Systems with Multibeam Antennas," *IEEE Proc. PIMRC*, pp.764-768, Sep. 1998.
- [6] Inoue, T. and Karasawa, Y., "Two-Dimensional RAKE Reception Scheme for DS/CDMA Systems in Beam Space Digital Beam Forming Antenna Configuration," *IEICE Trans. Commun.*, vol. E81-B, no.7, pp.1374-1383, July 1998.
- [7] Rappaport, T. S., *Wireless Communications: Principles and Practice*, 2<sup>nd</sup> Edition, New Jersey: Prentice Hall, 2002.
- [8] Azar, Y., Wong, G. N., Wang, K., Mayzus, R., Schulz, J. K., Zhao, H., Gutierrez, F., Hwang, D., Rappaport, T. S., "28 GHz Propagation Measurements for Outdoor Cellular Communications Using Steerable Beam Antennas in New York City," to appear in the *IEEE International Conference on Communications (ICC)*, June 9-13, 2013.
- [9] Rappaport, T.S., Murdock, J., Gutierrez, F., Jr., "State of the Art in 60-GHz Integrated Circuits and Systems for Wireless Communications," *Proceedings of the IEEE*, vol. 99, no.8, pp.1390-1436, Aug. 2011.
- [10] Gutierrez, F., Parrish, K., Rappaport, T.S., "On-Chip Integrated Antenna Structures in CMOS for 60 GHz WPAN Systems," *IEEE Journal on Selected Areas in Communications*, Vol. 27, Issue 8, pp. 1367-1378, October 2009.
- [11] Pi, Z., Kahn, F., "A Millimeter-wave Massive MIMO System for Next Generation Mobile Broadband," 46th Asilomar Conference, Nov. 2012.
- [12] Rappaport, T.S., Sun, S., Mayzus, R., Zhao, H., Azar, Y., Wang, K., Wong, G.N., Schulz, J.K., Samimi, M., and Gutierrez, F., "Millimeter Wave Mobile Communications for 5G Cellular: It Will Work!" *IEEE Access (Invited)*, Vol. 1, No. 1, pp. 335-349, May 2013.
- [13] MacCartney, G.R., Zhang, J., Nie, S., and Rappaport, T.S., "Path Loss Models for 5G Millimeter Wave Propagation Channels in Urban Microcells," accepted by *IEEE 2013 Global Communications Conference*, Dec. 9-13, 2013.
- [14] Colburn, J.S., Rahmat-Samii, Y., Jensen, M.A., Pottie, G.J., "Evaluation of personal communications dual-antenna handset diversity performance," *IEEE Transactions on Vehicular Technology*, vol.47, no.3, pp.737-746, Aug 1998.